A tropically hot mid-Cretaceous North American Western Interior Seaway

Jones et al. 2022

Supplemental Material

Additional supplemental material: Table S1 – Full geochemical data and details on specimen localities

ADDITIONAL SUMMARY PLOTS

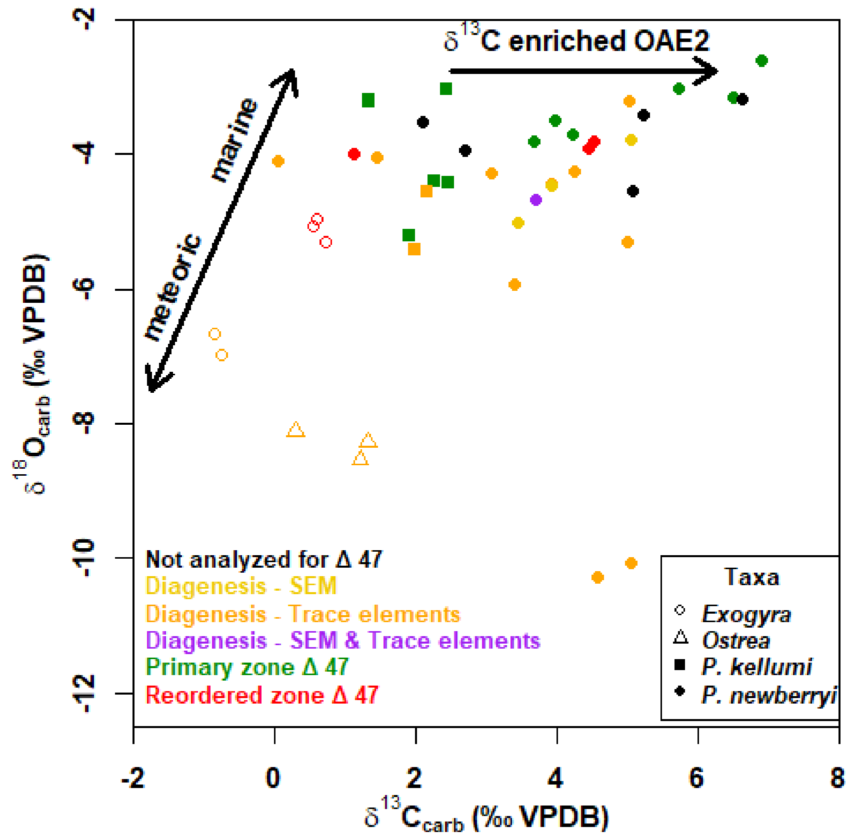

Figure S1. Cross-plot of stable carbonate carbon ($\delta^{13}C_{carb}$) and oxygen ($\delta^{18}O_{carb}$) isotope ratios of Cenomanian oyster specimens (n=43) on Vienna Pee Dee Belemnite (VPDB) and Vienna Standard Mean Ocean Water (VSMOW) scales. Red and green specimens passed diagenesis screening tests from SEM and elemental geochemistry and were analyzed for Δ_{47} geochemistry. Red specimens (n=6) are interpreted as likely experiencing reordering in geographic Zone 2 (see Fig. 1 and "Burial and Reordering Models" section below) and green specimens (n=11) are interpreted as preserving primary Δ_{47} geochemistry and paleotemperatures in Zones 1 and 3. Yellow, orange, and purple specimens failed one or both diagenesis screening tests (n=21). Black specimens passed elemental screening but were not selected for Δ_{47} analysis (n=5). Note - highly enriched $\delta^{13}C_{carb}$ values for most *P. newberryi* specimens (n=28) are consistent the taxon's range through the Oceanic Anoxic Event 2 (OAE2) interval, which was a time of relatively heavy $\delta^{13}C$ values. Lighter $\delta^{18}O_{carb}$ values reflect calcite precipitated from waters influenced by meteoric waters in the form of diagenesis or brackish water masses, whereas heavier $\delta^{18}O_{carb}$ values reflect calcite precipitated from more marine water masses. Note also that reordering (red points) does not affect the values of bulk $\delta^{18}O_{carb}$.

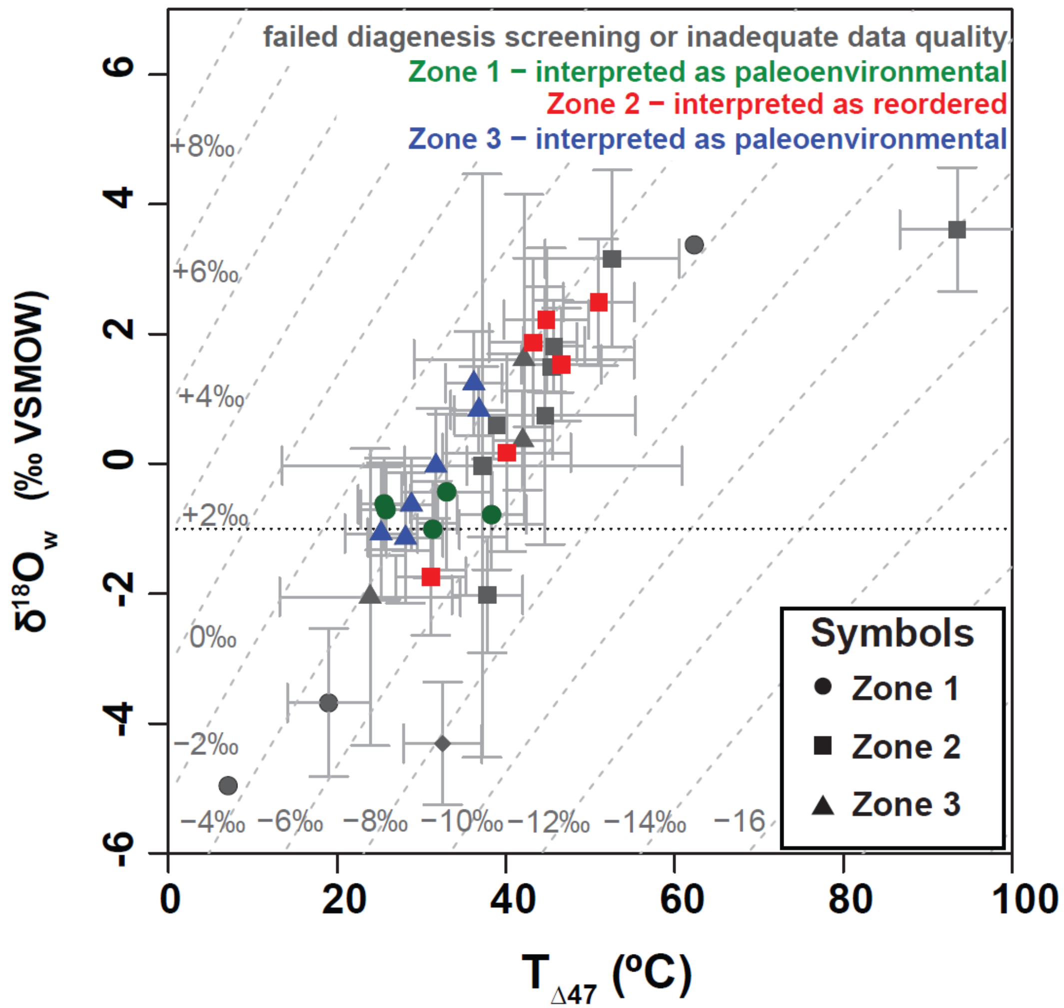

Figure S2. A cross-plot of all specimens measured for clumped isotope temperatures ($T_{\Delta 47}$) and oxygen isotope ratios of waters ($\delta^{18}O_w$) of precipitation, including diagenetically altered samples or those with poor data quality (gray symbols). The $\delta^{18}O_w$ values are calculated from $T_{\Delta 47}$ and measured oxygen isotope ratios of carbonate ($\delta^{18}O_{carb}$) using the equations of Kim and O'Neil (1997). Symbols correspond to geographic zone in the Western Interior Basin (see Figure 1). Colored markers show samples that were interpreted as not containing recrystallized calcite based on petrographic and elemental analyses. Gray text along dashed lines list $\delta^{18}O_{carb}$ values for specimens (Pee Dee Belemnite scale). One specimen (D5792-Pycnew), which failed diagenesis screening and was suspected of contamination, had extremely high temperatures (>400°C) and is not shown on this plot to preserve scale (Table S1). One altered specimen (D6899-OstC) marked by a diamond is from Texas (Table S1). See Figure 2 and the main text for full interpretations on $T_{\Delta 47}$ data.

ELEMENTAL ANALYSIS

Methodology: Diagenesis in meteoric settings commonly alters elemental contents of carbonates (Allan and Matthews, 1982; Veizer, 1983). To assess preservation of calcite for each macrofossil specimen, 2-10 mg of powder collected from the umbo area was weighed for elemental analysis. Powders were acidified in 2% HNO_3, centrifuged at 10,000 rpm for five minutes, and then analyzed on a Thermo Scientific iCAP Q ICP-MS in the Michigan Elemental Analysis Laboratory (MEAL) at the University of Michigan. Elemental contents were detected for Na, Mg, Si, S, K, Ca, Mn, Fe, Sr, Ba (2021 analyses), and Zn (2019 analyses) (Table S1).

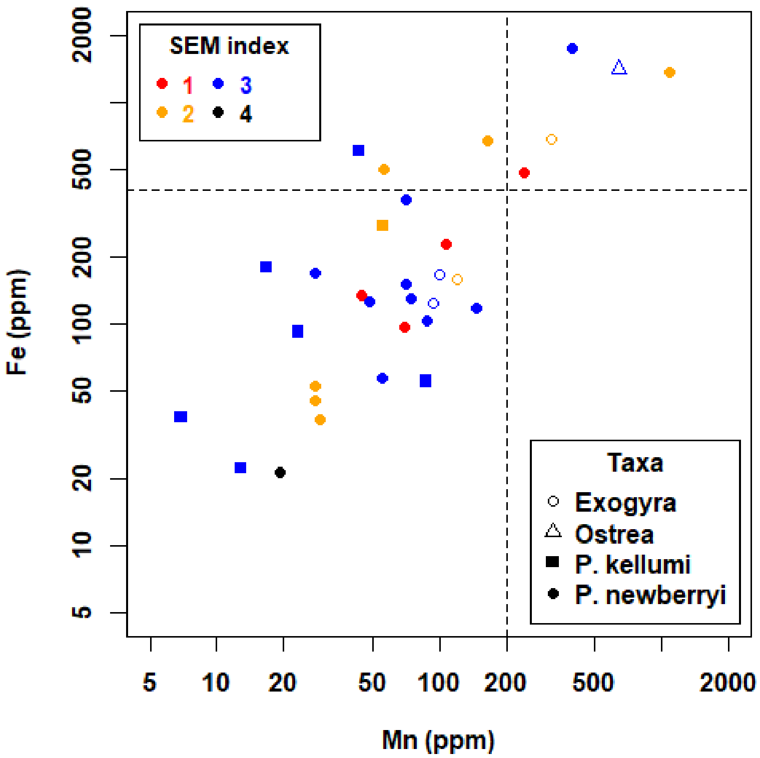

Figure S3. A cross-plot of iron and manganese abundances for powders drilled from the umbo region of oyster specimens. Colors correspond to SEM textural assessment of calcite preservation (see Table S2). Diagenetic calcite precipitated from meteoric waters is generally more enriched in Mn and Fe than in primary biogenic calcite (Veizer, 1983). Dashed lines represent cutoff criteria used to determine primary versus diagenetically altered calcite (Fe = 400 ppm, Mn = 200 ppm). A variety of elemental preservation cutoffs (e.g., Mn of 100-800 ppm) have been published for bivalves (Morrison and Brand, 1988; Voigt et al., 2003; Ullmann et al., 2013), including *Pycnodonte* (de Winter et al., 2018). Our thresholds within published ranges were selected considering the location of the main cluster of data as to avoid arbitrarily excluding a specimen with similar elemental composition to interpreted specimens. Some samples that fail the SEM assessment (SEM index < 2, Table S1) still have low Mn and Fe contents, indicating that growth of secondary calcites can also occur in low trace element environments and supporting the use of both screening methods together. Some discrepancies between SEM preservation and elemental contents also likely stem from the differing scale of each analysis. Whereas elemental analyses integrate over a larger homogenized drilled volume of the specimen (as much as 0.5 cm^3), SEM assesses internal mineral structures at scales as fine as tens of microns.

INFORMATION ON SPECIMENS

The specimens analyzed in this study were collected by William (Bill) Cobban of the USGS and colleagues from outcrops of the North American Western Interior Basin between 1957 and 1998. Specimens were formerly archived in the USGS Denver Fossil Collections until recently being transferred to the National Museum of Natural History at the Smithsonian Institution (McKinney and Cobban, 2018). Among the mollusk macrofossils from the Cretaceous Western Interior Seaway, Gryphaeidae oysters were selected for paleoclimate reconstruction in this study because they are extant at the family level, sessile, tolerate a wide range of environmental conditions, and have abundant low Mg calcite shell material that is resistant to diagenesis, making it suitable for Δ_{47} analysis. The suitability of Ostreida (oyster) macrofossils as geologic proxies for paleoclimatology and paleoceanography is founded on the premise that shell chemistry records ambient environmental conditions during growth. Modern adult oysters, of both the Ostreidae (true oysters) and Gryphaeidae (honeycomb or foam oysters) families, precipitate calcite in near isotopic equilibrium with seawater over wide ranges of salinity and temperature conditions, preserving geochemical profiles in shells that track sub-annual environmental changes (Kirby et al., 1998; Surge et al., 2001; Ullmann et al., 2010; Titschack et al., 2010; Huyghe et al., 2020). Additionally, the sessility of adult Ostreida provide stationary paleoenvironmental records and avoid the complications of interpreting geochemical signals from free-swimming taxa that migrate through different water masses (e.g., Linzmeier, 2019). Proxies based on macrofossil geochemistry also rely on the assumption that primary shell mineralogy is retained post-deposition. Gryphaeidae fossils of the genus *Pycnodonte*, which are analyzed extensively in this study, consist of interlayers of dense foliated calcite and porous chalky calcite, the latter of which is susceptible to diagenetic calcite accumulation in pores (de Winter et al., 2018). Therefore, we collected sample powders from the umbo region of the macrofossils, where foliated layers are denser and infilling diagenetic calcite is less likely to be encountered. Additionally, we screen samples for carbonate diagenesis using SEM imaging (Table S2) and elemental abundances (Fig. S3; Table S1c).

Shallow marine sediments deposited by the Cenomanian-Turonian Greenhorn Cyclothem of the Western Interior Seaway preserve a rich faunal record (Kauffman & Caldwell, 1993). Cenomanian oysters from the seaway have been collected and described in detail by paleontologists (Stanton, 1893; Jones, 1938; Cobban, 1977; Kauffman and Powell, 1977; Elder, 1991; Kirkland, 1996; Sealey and Lucas, 2003). These expeditions have refined taxonomy and developed a biostratigraphy for Ostreida in the seaway (Hook and Cobban, 1977; Kauffman et al., 1993). Ranges for the taxa are constrained by regional lithostratigraphy, ammonite biostratigraphy, radioisotopically dated bentonites, and in some cases carbon isotope chemostratigraphy (e.g., Elder, 1987) (Figure S4). In the case of the *Pycnodonte* specimens analyzed, *Pycnodonte newberryi* (formerly *Gryphea newberryi*) is an index fossil for the Late Cenomanian interval that corresponds to Oceanic Anoxic Event 2. *P. newberryi* appears to have evolved from a lineage endemic to the WIS, progressing from the ancestral Middle to earliest Late Cenomanian *Pycnodonte kellumi* (*Pycnodonte cf. P. Kellumi*), to an early Late Cenomanian intermediate species *P. n.sp.* (*P. aff. P. kellumi*), and ultimately to the Late Cenomanian *Pycnodonte newberryi* through the OAE2 interval (Hook and Cobban, 1977). In this study, we do not differentiate between the closely related *P. kellumi* and *P. n.sp.* due to ambiguities in collection notes and subsequent changes in taxonomic designations of these two specimens, but all are distinguished from *P. newberryi* and therefore are grouped into the pre-OAE2 interval.

Pycnodonts primarily favored hard substrates for colonization and are restricted to offshore facies, apparently absent in shallowest marine facies (Kauffman, 1967; Kirkland, 1996). They commonly occur in thick bioherms that mark relative sea level transgressions and siliciclastic starvation (e.g., Elder, 1991). However, Hook and Cobban (1981) also contended that the Pycnodonts were better adapted than other bivalves in the seaway to colonize soft substrates as well, which may contribute to their abundance in the siliciclastic-rich southwestern margin of the WIS.

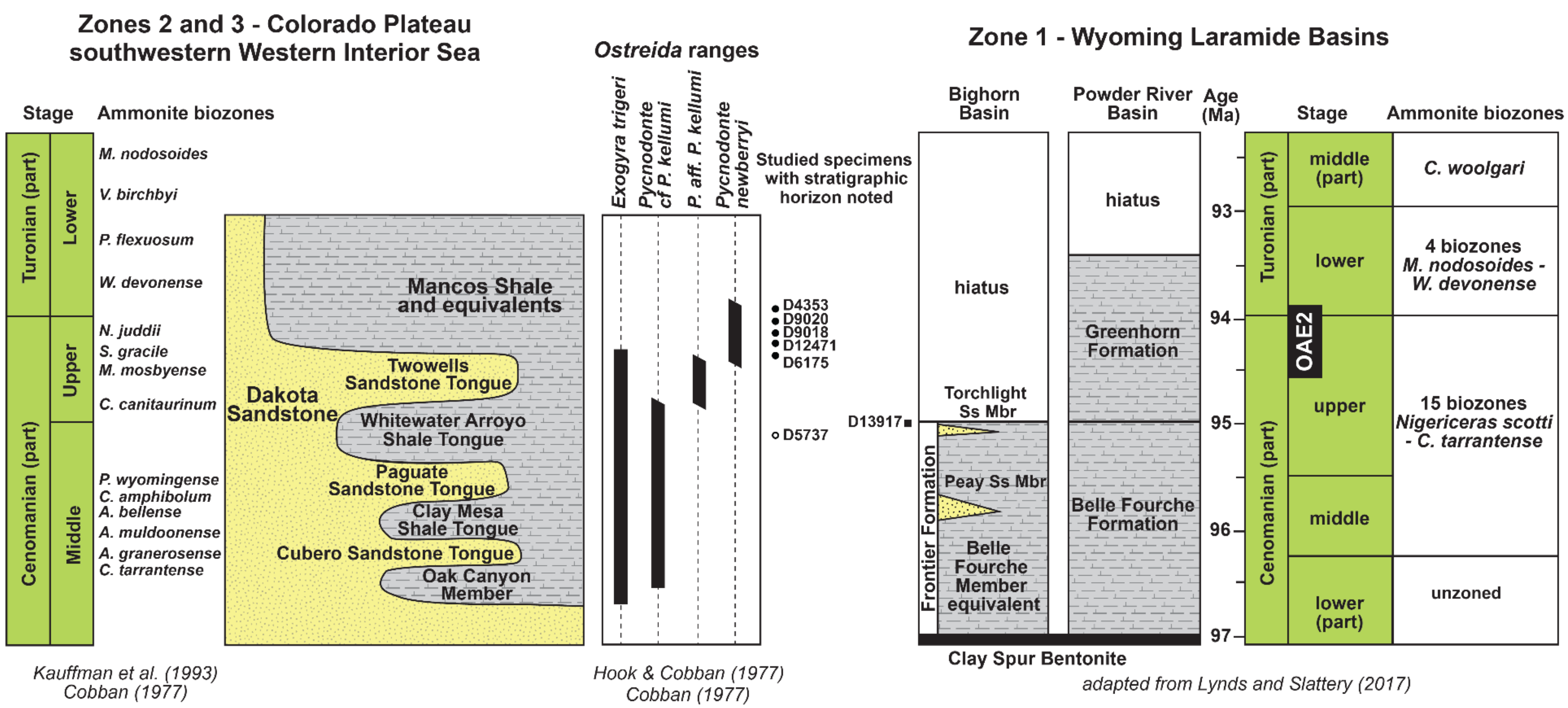

Figure S4. Generalized stratigraphy of the Western Interior Seaway in Zones 1 (Wyoming) and Zones 2 and 3 (Colorado Plateau), including biostratigraphic ranges of studied Cenomanian *Ostreida* specimens. Where available, the stratigraphic horizons for original collection of specimens are displayed for the specimens analyzed for $T_{\Delta 47}$ in Fig. 2. Not all archived specimens had stratigraphic information preserved (see full details in Table S1c). For those specimens, the uncertainty on their stratigraphic horizon/ages is considered to be the full biostratigraphic range for the region (specimens D8407, D8304, D11792, D2052, D11889).

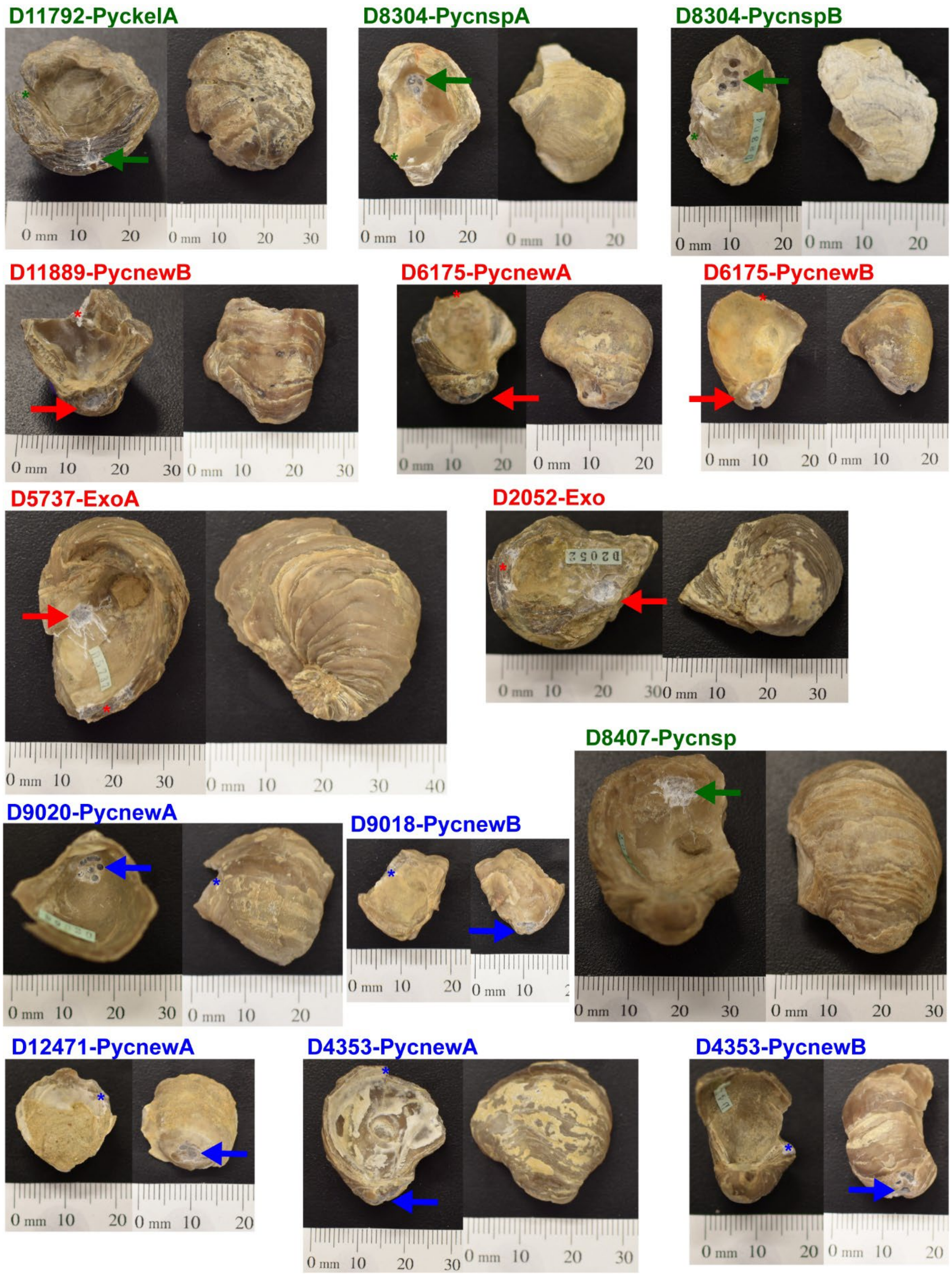

Figure S5. Photos of select specimens analyzed. Arrows show sampling for Δ_{47} analyses and asterisks show sampling for SEM. Colors correspond to specimens' geographic zones in Fig. 1.

SCANNING ELECTRON MICROSCOPY (SEM)

Methodology: All specimens were assessed for carbonate preservation quality using a JEOL JSM-7800FLV field-emission scanning electron microscope (SEM) at the Electron Microbeam Analysis Lab at the University of Michigan. We broke off two pieces of shell from near the ventral margin of a single valve, mounting one piece flat and the other piece at a 45° angle on the stub to image the exterior surface and an oblique cross-sectional view of the fractured surfaces. After mounting, a light stream of compressed air was blown across the sample surface to remove debris resulting from the breakage that would overlay the surface and potentially accumulate noise. Samples were carbon-coated and examined under SEM at an accelerating voltage of 10 kV and at magnification ranging from 100x to 5000x.

Table S2. SEM Preservation index for specimens.

Preservation index	Description
5 (see Lee et al., 2011 and Checa et al., 2018)	**No evidence of secondary mineralization or dissolution.** The foliated layer is made of clearly defined laths with readily definable orientations. Boundaries between folia and prisms are clear and well-defined. Indistinguishable from modern oysters
4 (Fig. S6A,B)	**No evidence of secondary mineralization.** Some evidence of minor dissolution near the surface, but deeper layers are pristine. Primary microstructures including folia and prisms are identifiable and boundaries well-defined throughout the shell.
3 (Fig. S6C,D)	**No evidence of secondary mineralization.** Dissolution features may be moderate near the surface, but deeper layers show only minor dissolution. Primary microstructures including folia and prisms are readily identifiable, but boundaries may be slightly irregular due to dissolution.
2 (Fig. S6E,F)	**No evidence of secondary mineralization.** Dissolution features are moderate near the surface and at depth. The directionality of primary microstructures including laths of the foliated layer and prisms is visible, but boundaries are poorly defined where observed. Preservation quality may be mixed in different areas of the shell.
1 (Fig. S6G,H)	**Minor to severe evidence of secondary mineralization and fusion of adjacent layers.** Moderate to severe dissolution features persist at depth. Significant to complete loss of directionality and distinct boundaries in laths of the foliated layer and prisms. Preservation quality may be mixed in different areas of the shell.

Preservation assessment: We developed a new preservation index (PI) scale (Table S2) to rank preservation quality of the oyster calcite from 1 (poor) to 5 (pristine). The PI scale presented here was modeled after aragonite preservation rubrics developed by Cochran et al. (2010) and Knoll et al. (2016) for Late Cretaceous mollusk shells from the Western Interior Basin. Like those examples, we base the PI ranking on the clarity of major microstructural features (for these calcitic oysters, folia consisting of radiating laths and a prismatic layer) and extent of dissolution. The criteria listed in Table S2 heavily weight diagenetic artefacts known to influence clumped isotope analysis, namely recrystallization or secondary mineralization. The severity of dissolution was ranked from minor to severe based on the depth at which it persists in the cross section of the shell fragment, the degree to which they obscured the orientation and boundaries of laths and prisms, and an estimation of the total surface area of the shell fragment affected.

We conservatively assign any sample with clear evidence for secondary mineralization (e.g., calcitic infilling, fusion of layers, amorphous overgrowths, blebs) a PI of 1 regardless of the state of dissolution in other areas of the shell, although secondary mineralization was often also accompanied by more advanced dissolution features (e.g., etching, microborings). All shells with a PI of less than 2 were excluded from the final dataset. Some samples assigned a PI of 2 saw moderate-to-severe dissolution or inconclusive evidence of minor reprecipitation in one area of the fragment, but preservation that would rank ≥ 3 in other areas. Shells receiving a PI of 2 were not automatically excluded from the dataset because preservation quality demonstrably varied in space and the fragments themselves were taken far from the site of geochemical sampling. In these cases, the decision to include or exclude a shell from the dataset was made based on the thresholds set for Fe and Mn content.

Figure S6 (following page). SEM images representing preservation index values. A) Foliated layer of *Pycnodonte newberryi* (PI = 4) in specimen D12471-PycnewB with well-defined laths and foliation. B) Alternate view of foliated layer of specimen D12471-PycnewB. C) Foliated layer of *Pycnodonte newberryi* (PI = 3) in specimen D9020-PycnewB with orientation of laths and folia discernable, but boundaries made less distinct from dissolution. D) Foliated layer of *Exogyra* (PI = 3) in D5737-ExoB showing minor dissolution, but clear orientation and boundaries of laths and folia. E) Foliated layer of *Pycnodonte newberryi* (PI = 2) in specimen D4353-PycnewB with orientation of laths somewhat discernable, but with very poorly defined boundaries. F) Foliated layer of *Pycnodonte kellumi* (PI = 2) in specimen D13917-PyckelB with orientation of laths somewhat discernable, but with very poorly defined boundaries. Dissolution is more severe, and some layers of folia appear to be fused. G) Foliated layer in *Pycondonte newberryi* (PI = 1) in specimen D5792-PycnewB with all major microstructural features obscured by apparent dissolution and reprecipitation. H) Cross-sectional view of *Pycnodonte newberryi* (PI = 1) in specimen D7361-PycnewA with no discernable layering or other readily identifiable microstructure. Scale bars represent 20µm. Images were adjusted for brightness in Adobe Photoshop 2020.

198

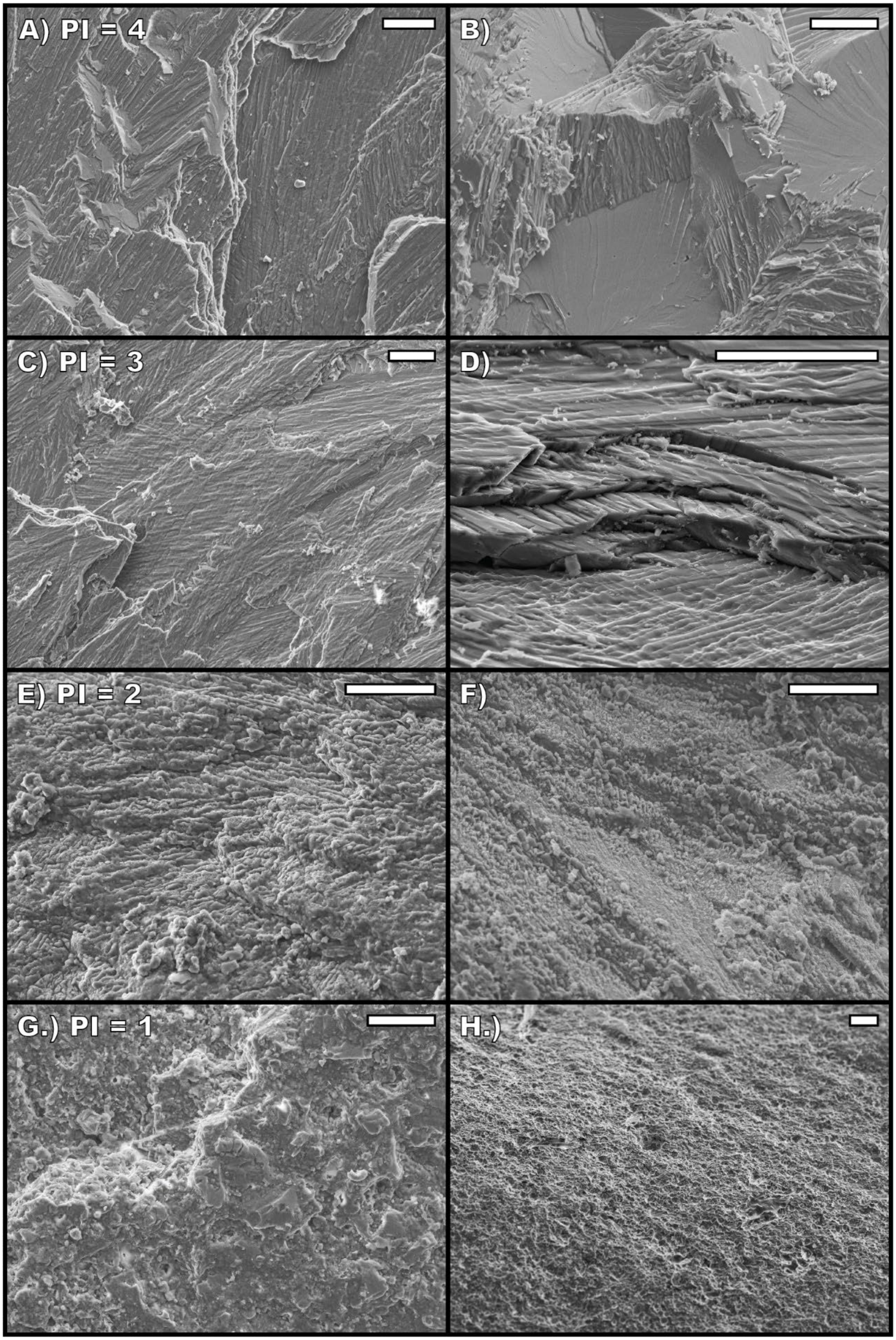

CLUMPED ISOTOPE ANALYTICAL METHODS

Powders of the oyster macrofossils were measured for carbonate clumped isotope and stable isotope values in the Stable and Clumped Isotopes for Paleoclimate and Paleoceanography (SCIPP) laboratory at the University of Michigan during several measurement sessions between 2015 and 2020. Analytical procedures follow Petersen et al. (2016) and Meyer et al. (2018) described below.

MAT 253 Δ_{47} analyses (2015-2019). Sample powders of 3.5-4.5 mg were acidified on a manual gas extraction line in a common acid bath of anhydrous H_3PO_4 at 75°C for at least 15 minutes and until effervescence ceased. Water and incondensable gases were removed from the evolved CO_2 using a -90 to -95°C isopropanol trap and liquid nitrogen (LN_2) pump overs. Additional potential contaminants were removed using a Porapak (PPQ) trap cooled to -12 to -15°C, which were baked for 30 minutes prior to usage. Purified aliquots of CO_2 were analyzed on a Thermo MAT 253 dual inlet isotope ratio mass spectrometer. Each gas was analyzed for approximately 2 hours at ~15V intensity on the m/z 44 peak for 12 cycles and 5 acquisitions (60 cycles total), bracketed by measurements of the laboratory's working reference gas. Intensities of m/z 45-49 were ratioed to m/z 44 intensity and raw Δ_{47} values were calculated. Values of $\delta^{13}C$, $\delta^{18}O$, and Δ_{47} were calculated from raw intensities on faraday cups using the updated ^{17}O abundance parameters from Brand et al. (2010) (Petersen et al., 2019). In addition to our sample gases, we also measured gases from in-house carbonate standards for the SCIPP lab including Carrara Marble, Joulers Cay Ooids, and CORS (shallow water coral, Rosenheim, 2013).

Nu Carb-Nu Perspective Δ_{47} analyses (2021). A second round of sample powders were analyzed for Δ_{47} geochemistry on a Nu Carb automated carbonate preparation device connected to a Nu Perspective dual-inlet mass spectrometer. Powders (~4 mg) were acidified in 150µL of anhydrous H_3PO_4 at 70°C for 20 minutes. Evolved gases were collected in a -160°C LN_2 trap that was next warmed to -60°C, retaining H_2O and transferring CO_2 for 800 seconds through a -30°C Porapak Type Q trap to a second LN2 trap, removing additional contaminants. Following a pump over to remove incompressible gases (N_2, Ar), the second LN_2 trap was warmed to -60°C to retain any residual water and the purified sample CO_2 gas was expanded into the sample side bellows. To increase gas pressure and achieve a beam strength of $8x10^{-8}$nA on the m/z 44 faraday cup for both reference and sample gases, bellows were incrementally compressed between each measurement cycle. Intensities of m/z 44-49 Faraday cups were measured as sample-reference gas pairs for 4 blocks of 20 cycles. Raw intensities from the Nu Perspective were converted to values of $\delta^{13}C$, $\delta^{18}O$, and Δ_{47} using the same approach as for the MAT 253 (see above). The same set of in-house standards analyzed on the MAT 253, along with newer *Arctica Islandica* (Ice) and *Cittarium Pica* in-house standards, were measured on the Nu Perspective to ensure accurate calibrations and consistent geochemical results between instruments.

Calibration: Interactions within the mass spectrometer lead to a δ^{47}-Δ_{47} nonlinearity in raw Δ_{47} values, potentially from the generation of secondary electrons (Fiebig et al., 2016). This source "scrambling" overprint of clumped isotope ratios (Huntington et al., 2009) changes in character over the course of weeks to months depending on the performance and conditions of a given mass spectrometer. To account for instrument mass fractionation during the MAT 253 analyses, we measured at least six standard gases per week of CO_2 equilibrated with water at 25°C and CO_2 heated to 1000°C, both of which have known Δ_{47} values defined based on thermodynamic constraints (Wang et al., 2004). For analysis sessions on the Nu Perspective, we measured "ETH" carbonate standards and assigned values from the "Intercarb" project (Bernasconi et al., 2021) along with a smaller number of heated and equilibrated gases. These standards were used to construct empirical transfer functions (ETF) and convert raw Δ_{47} values to absolute reference frame Δ_{47RF} values for a given time window (Dennis et al., 2011). Boundaries of windows for the various ETFs used were selected at break points between measurement sessions, temporary instrument shutdowns, and when raw Δ_{47} values of gas standards abruptly shifted. The mean slope of the equilibrium gas lines (EGL: raw Δ_{47} vs δ^{47}) for measurement sessions on the Nu Perspective (0.001388) was an order of magnitude less than the mean EGL slope for sessions on the MAT 253 (0.021479). This reflects better shielding of faraday cups from secondary electrons and other interferences in the newly installed Nu Perspective. Δ_{47RF} values were then corrected for fractionation during acid digestion to the conventional reference reaction at 25°C ($\Delta^*_{25\text{-}75}$: Bonifacie et al., 2017), using a value of 0.072 for samples from the MAT-253 reacted at 75C or 0.066 for samples from the Nu reacted at 70°C (Petersen et al., 2019). The accuracy of final Δ_{47rfac} data within each calibration window was evaluated based on results of the in-house carbonate standards. Using the composite calibration of Petersen et al. (2019) (slope = 0.0383 ‰/10^{-6}/T^{-2}, intercept = 0.258‰), Δ_{47} temperatures ($T_{\Delta47}$) were derived for the average $\Delta_{47\text{-}RFAC}$ value of all replicates. We also apply the recent Δ_{47} calibration of Anderson et al. (2021) and calculate associated values of $\delta^{18}O_w$. Using this calibration, $T_{\Delta47}$ of non-diagenetically altered specimens are systematically 2.4- 3.8°C cooler than the Petersen et al. (2019) calibration and $\delta^{18}O_w$ values are 0.48 to 0.63‰ (VSMOW) lighter (Table S1d).

Quality assurance: At least 3 replicates analyses per powder were measured to quantify sample level summary statistics, including mean and standard error values for Δ_{47} compositions and $T_{\Delta47}$ for specimens. Note, replicates for each powder analysis were measured on the same instrument (i.e., either the MAT 253 or Nu Perspective). Replicates with anomalously high Δ_{48} values on the MAT 253 were interpreted to reflect contamination and were not considered further. Some of these were reanalyzed on the Nu, which more successfully removed Δ_{48} anomalies down to gas-standard-baselines, also resulting in $T_{\Delta47}$ in better agreement with other samples, supporting interpretations of contamination in earlier samples. Internal and external standard error (SE) were reported for Δ_{47} measurements and associated calculations. Internal SE equals the standard deviation of Δ_{47} replicates for a sample powder divided by the square root of the number of replicates: (internal SE = $1\sigma_{sample}$/sqrt(N)). External SE equals the long-term standard deviation of standard reference material in the SCIPP Lab for the MAT 253 ($1\sigma = \pm0.025$‰) and Nu Perspective ($1\sigma = \pm0.015$‰) divided by the square root of the number of replicates (N). Error bars in figures reflect the greater value between internal SE and external SE for a given specimen. $\delta^{18}O$ values of water ($\delta^{18}O_w$) in the Cretaceous Western Interior Seaway were calculated using $T_{\Delta47}$–the Δ_{47} derived temperature of calcite precipitation–and $\delta^{18}O_{carb}$ following the calcite equation of Kim and O'Neil (1997). The uncertainty for $\delta^{18}O_w$ values was calculated by propagating the ±1 SE of the $T_{\Delta47}$ data (internal or external, whichever was greater) along with the ±1 SE from $\delta^{18}O_{carb}$ data.

BURIAL AND REORDERING MODELS

The original clumped isotope geochemistry of carbonate minerals can be altered by post-depositional solid-state bond reordering if samples are subjected to elevated temperatures for prolonged periods of time (Passey and Henkes, 2012; Henkes et al., 2018). For mid-Cretaceous aged specimens, 1% partial reordering has been modeled to begin at thresholds of between ~80-100°C (Henkes et al., 2014; Stolper and Eiler,2015; Hemingway and Henkes, 2021). Thus, in addition to diagenetic screening, the thermal history of specimens must be considered when interpreting carbonate clumped isotope paleothermometry data. However, since any thermal history model must necessarily make many assumptions (burial depth through time, geothermal gradient through time, differing models for reordering kinetics, etc.), this is a more qualitative approach that can inform whether reordering may have occurred and the magnitude of any $T_{\Delta47}$ reordering shift.

Zone 1 (Wyoming): The data presented in this study originate from three geographic zones with distinct burial histories (Fig. 1). For the five pre-OAE2 mid-late Cenomanian specimens assessed to preserve primary calcite from the Frontier Formation in Wyoming (Zone 1), the $T_{\Delta47}$ is 26-35°C (95% CI: confidence interval on the standard error of the mean). This stratigraphic unit is a thermally mature source rock in the center of Laramide basins, like the Wind River Basin. However, at many outcrops where the oyster specimens were collected, low vitrinite reflectance values indicate a comparatively shallow burial history along basins' margins (Nuccio et al., 1996). Apatite (U-Th)/He thermochronology data from the Bighorn Mountains indicate low thermal burial conditions for the range itself (Crowley et al., 2002), implying low thermal maturity zones along the margins of the Wind River and Powder River basins. In particular, two explanations listed by Crowley et al. (2002, p. 29) are:

> "(1) Pre-Laramide sedimentary cover over the basement was thinner than suggested by evidence from adjacent basins. (2) The geothermal gradient was extremely low (<20°C/km)…"

Given the spatial gradients in thermal maturity of the Frontier Formation from Laramide basins' centers to margins, it is challenging to reconstruct a precise time-$T_{\Delta47}$ pathway from a widely representative stratigraphic column. However, if we utilize (U-Th)/He thermochronology data from the Bighorn Mountains, which found a ~20°C/km geothermal gradient and 1.5 km of Cretaceous subsidence/sedimentation (see Fig. 2 in Crowley et al., 2002), as well as assume that adjacent Cretaceous outcrops experienced a similar thermal history, we can test reordering kinetic models for our Zone 1 specimens (Fig. S7). Since this burial pathway would generate low maximum burial temperatures (~60°C) below all modeled thresholds for Δ_{47} reordering (Hemingway and Henkes, 2021), we interpret $T_{\Delta47}$ values from Zone 1 as primary records of mid-Cretaceous climate. Further, $T_{\Delta47}$ of specimens from Wyoming (Zone 1) are reasonable and only 1 of 6 specimens were screened based on other diagenesis metrics, consistent with a mild burial history and an interpretation of primary $T_{\Delta47}$ values. In general, it appears Cretaceous outcrops (and perhaps pre-Cretaceous) from the margins of Laramide basins in northern Wyoming, and potentially nearby areas (e.g., Gao et al., 2021), are promising prospective targets for future Δ_{47} paleotemperature studies in North America.

Zone 3 (central Colorado Plateau): For the Cenomanian specimens analyzed in this study from the central Colorado Plateau (Zone 3), we can infer a range of burial conditions based on the stratigraphic thickness and ages of overlying strata from the Grand Staircase of southern Utah. Local observations suggest moderate thermal conditions, including limited clay mineral diagenesis

(Nadeau and Reynolds, 1981), immature organic matter (Boudinot et al., 2020), preservation of primary hydrogen isotope ratios of kerogen (Todes et al., 2017), and subbituminous grades of local coal (Hettinger, 2001). In particular, recent apatite fission-track (AFT) thermochronologic data from the Kaiparowits Plateau of the Grand Staircase provide more precise thermal history constraints for Zone 3 (Murray et al., 2019). The AFT data indicate that, aside from aureole zones within several kilometers of regional volcanic features (e.g., Henry Mountains), Zone 3 has remained cooler than the AFT closure temperature window of 140-90°C since before the Cenomanian. This indicates that our oyster fossils have likely remained cooler than or very close to the lowest thermal thresholds for Δ_{47} reordering. Based on these observations and the limited number of specimens identified as diagenetically altered (2 of 8 specimens), we consider it unlikely that Δ_{47} geochemistry in Zone 3 was affected by substantial burial driven reordering similar to Zone 1.

Because of the availability of well constrained unit thicknesses for the stratigraphic column of the Grand Staircase, we can estimate the magnitude of possible reordering due to the estimated burial history. Assuming a typical geothermal gradient of 25˚C/km, maximum burial temperatures for Cenomanian strata would have approached ~80-100˚C in the Eocene (Table S3). Kinetic Δ_{47} reordering models by Henkes et al. (2014) and Hemingway and Henkes (2021) indicate that such time-temperature paths are insufficient to substantially alter $T_{\Delta47}$ (Fig. S9 A-D). The model presented by Stolper and Eiler (2015) predicts a mean change in $T_{\Delta47}$ of ~+3˚C from reordering for the shallow burial scenario (Fig. S9C) and ~+35°C for the deeper burial scenario. The latter scenario would generate altered values $T_{\Delta47}$ of ~40-80°C, which are not observed in Zone 1. Given equivalent $T_{\Delta47}$between Zone 3 and Zone 1, and many independent lines of evidence for relatively low burial temperatures in the central Colorado Plateau (see above), our data are most consistent with a typical geothermal gradient for Zone 3 (sites: D12471, D4353, D9018, D9020) in line with local AFT thermochronology data. As a result, we interpret the Δ_{47} data for specimens with primary calcite from the central Colorado Plateau (Zone 3) as annually-averaged paleotemperatures and $\delta^{18}O_w$ values of water from the WIS, and include a caveat that a scenario of low-level, single-digit ˚C reordering cannot be entirely dismissed given these reconstructed burial conditions. Regardless, relatively minor reordering in $T_{\Delta47}$ in Zone 3, such as original temperatures several degrees C lower than measured, would not alter our overarching interpretation of an extremely hot WIS in the mid-Cretaceous.

Zone 2 (margins of Colorado Plateau): Conversely, samples from sites along the periphery of the Colorado Plateau to the south and east (Zone 2) show $T_{\Delta47}$ of 37-48°C (95% CI) which may indicate a higher degree of reordering than in the central or western Colorado Plateau due to local volcanic features and burial histories (Figs. 1 and 3). In contrast to Zone 3, there is no stratigraphic column of characteristic thickness for Zone 2, and the area is more structurally complex with a higher potential for post-depositional heating due to local Cenozoic volcanism. Specimens in Zone 2 that pass diagenetic screening have temperatures that are significantly (two sample t-test, p-value < 0.01) ~10°C warmer than specimens from Zone 3 to the west. This amount of warming is consistent with a scenario where the Cenozoic geothermal gradient was steeper or burial depth was greater in Zone 2 than in Zone 3 (e.g., Fig. S9b, 7d, 9f). Separately, existing heat flow and thermal maturity models for the mid-Cretaceous strata in the region reflect higher thermal maturity towards the center of the Western Interior Basin in general (Nadeau and Reynolds, 1981; Law, 1992; Dumitru et al., 1994; Nuccio and Condon, 1996; Pancost et al., 1998; Flowers et al., 2008; Pacheco, 2013, pgs. 48-75). Additionally, 7 of 14 specimens from this zone were deemed diagenetically altered based on SEM and trace element thresholds. Many of these diagenetically altered samples also preserve even higher $T_{\Delta47}$, greater than 50°C (e.g., D6816-PycnewB-Nu: 93.5°C, D10440-PycnewA: 52.6°C, D5792-PycnewB: 431°C). We interpret this significant west to east increase in $T_{\Delta47}$ of latest Cenomanian specimens to result from solid-state reordering, a phenomenon that appears to be consistent with reordering in Zone 2, as well as poorer carbonate preservation in general. Therefore, we conclude that samples from Zone 2 have likely experienced minor to moderate reordering, and that the $T_{\Delta47}$ values no longer reflect paleoceanographic temperatures. Whereas Zone 1 and Zone 3 have milder burial conditions and seem to preserve primary paleoenvironmental signals. Interestingly, in the case of reordering, Δ_{47} changes but $\delta^{18}O_{carb}$ does not (Fig. S1). If we combine $\delta^{18}O_{carb}$ values from Zone 2 with the mean temperature from Zone 3, the resulting mean $\delta^{18}O_w$ value for Zone 2 shifts to -1.1‰ (VSMOW). This value is is consistent with Cretaceous seawater and the $\delta^{18}O_w$ values found from Zones 1 and 3, as well as from offshore marine facies in younger, more shallowly buried strata of the WIS (see Fig. 4). This further supports an interpretation of generally mild (<10°C), but non-negligible reordering of $T_{\Delta47}$ values of biogenic carbonates in Zone 2.

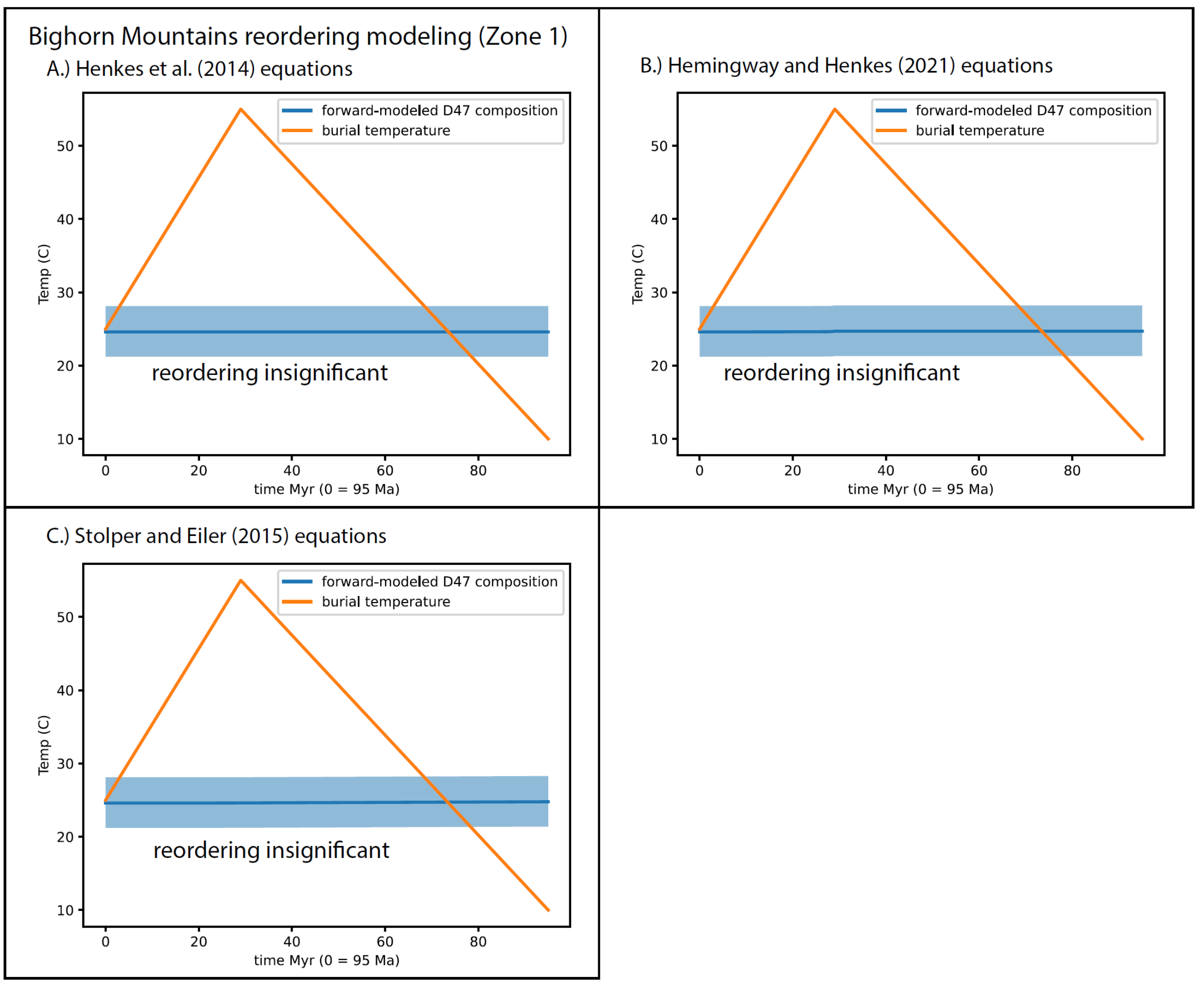

Figure S7. Results of clumped isotope solid state reordering models for Zone 1 Cenomanian calcite from the margins of Laramide Basins in northern Wyoming based on apatite thermochronology of the Bighorn Mountains (Crowley et al., 2002). Calculations and figures are output from the open source 'isotopylog' module written in python and test three different sets of equations (Hemingway, 2020; http://pypi.python.org/pypi/isotopylog).

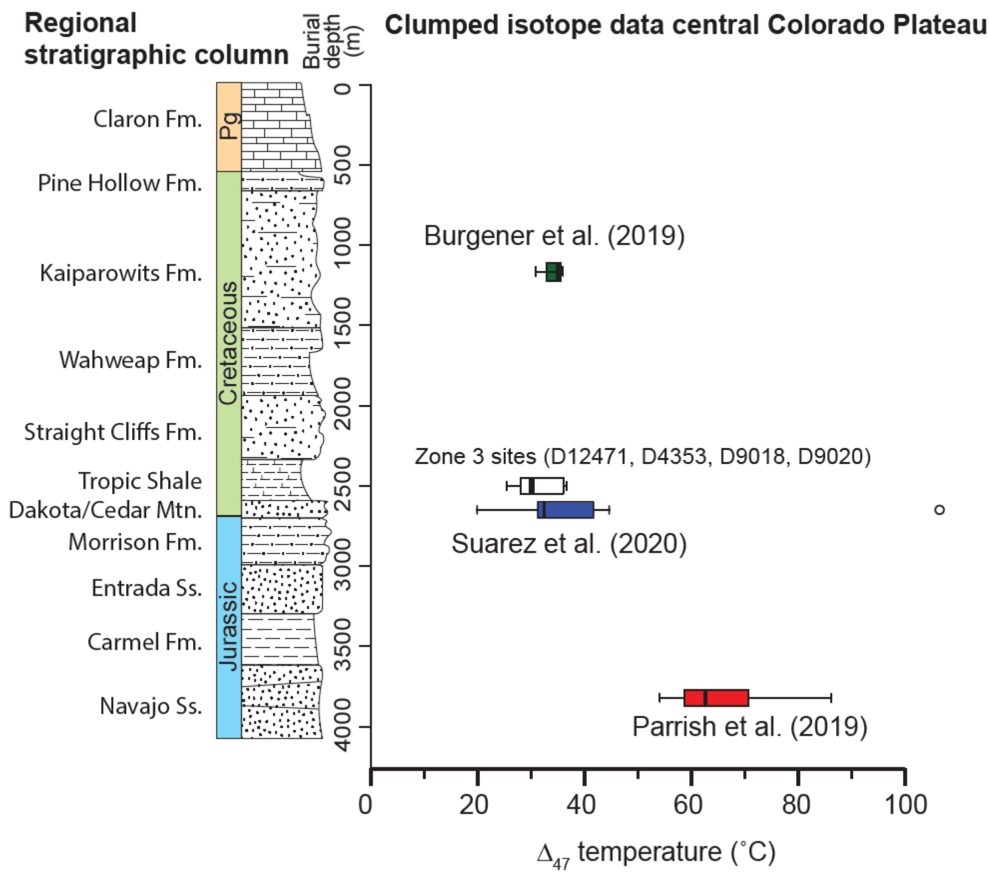

Figure S8. Stratigraphic column of the Grand Staircase in southern Utah with box and whisker plots of clumped isotope paleotemperature ranges from several formations in the area of Zone 3 from this study. Locally, $T_{\Delta 47}$ data from the Navajo Sandstone (Parrish et al., 2019) indicate that significant reordering occurs stratigraphically lower than the studied marine Cenomanian Tropic Shale Formation, along with the terrestrial Aptian-Albian Cedar Mountain Formation (Suarez et al., 2020) and Campanian Kaiparowits Formation (micritic paleosol nodules of Burgener et al., 2019). This compilation also supports recent findings from the Green River Basin (Wyoming, USA) that place the regional burial threshold for Δ_{47} reordering at ~3km (Lacroix and Niemi, 2019).

Table S3. A generalized thermal history for the central Colorado Plateau from the stratigraphy of the Grand Staircase in southern Utah, regionally corresponding to our specimens from Zone 3 localities. Burial depth and timing inferred from first-order ages and stratigraphic thicknesses of local formations (Fm.) (Bower, 1972; Titus et al., 2005). Maximum and minimum burial temperatures (T) are calculated assuming a geothermal gradient of 25°C/km.

Age (Ma)	Time (Myr)	Min. burial (m)	Max. burial (m)	Min. T (25°C/km)	Max. T (25°C/km)	Event
0	95	0	0	10	10	Exhumation
51	44	2301	3110	83	103	Claron Formation
57	38	1798	2516	70	88	non-deposition
59	36	1798	2516	70	88	Pine Hollow Formation
61	34	1798	2394	70	85	non-deposition
64	31	1798	2394	70	85	Canaan Peak Fm.
67	28	1698	2089	67	77	non-deposition
74	21	1698	2089	67	77	Kaiparowits Fm.
76	19	843	1234	46	56	Wahweap Fm.
81	14	483	774	37	44	Straight Cliffs Fm.
91	4	183	274	30	32	Tropic Shale Fm.
95	0	0	0	25	25	Dakota Sandstone

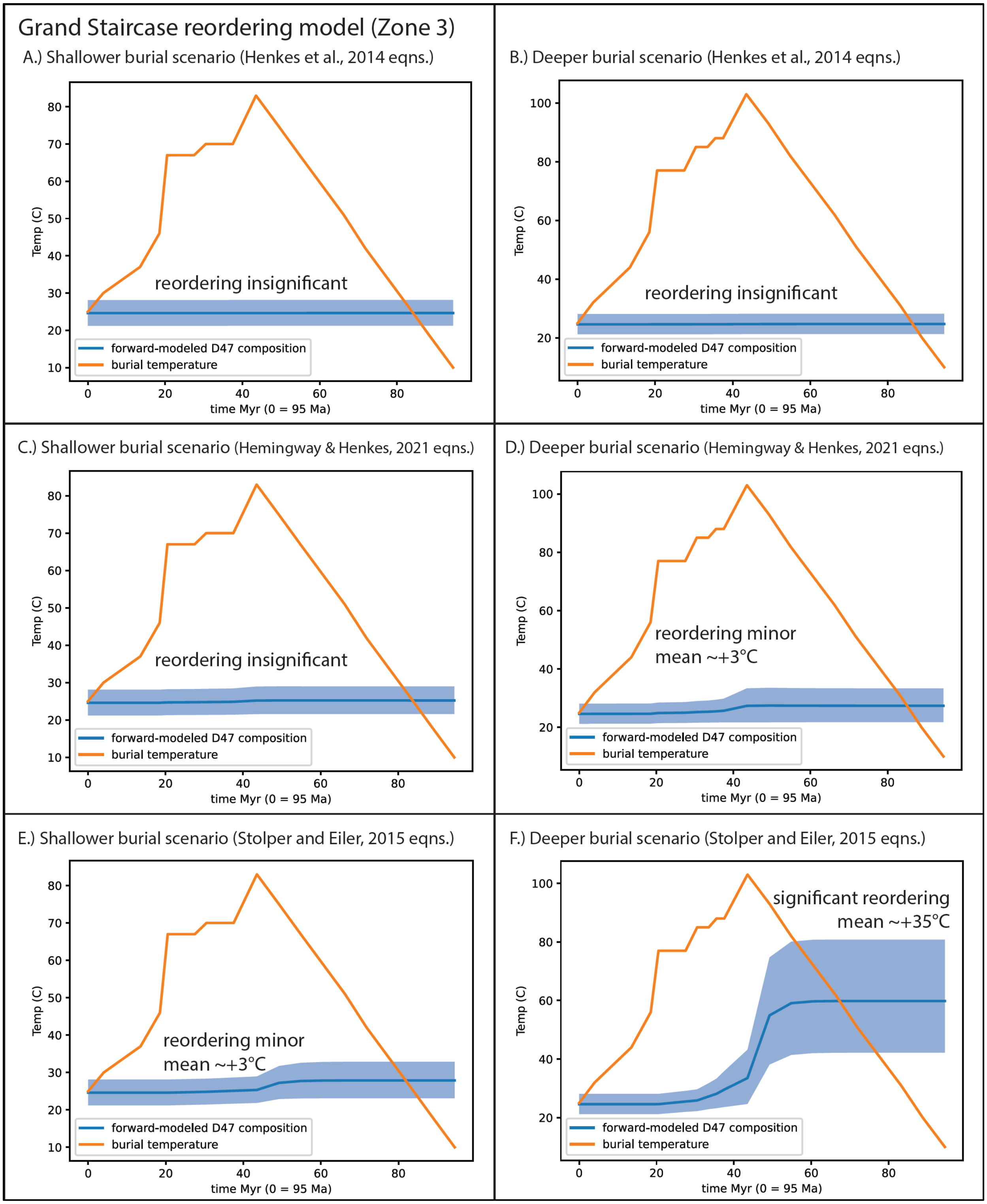

Figure S9. Results of clumped isotope solid state reordering models for calcite in Cenomanian strata from the central Colorado Plateau near the Grand Staircase of southern Utah, representing specimens from Zone 3. Calculations and figures are output from the open source 'isotopylog' module written in python (Hemingway, 2020; http://pypi.python.org/pypi/isotopylog). Zero time is equivalent to 95 Ma and initial calcite temperatures are set to ~25°C to test whether calcite precipitated in a warm time interval is significantly altered under different hypothesized burial scenarios. Results are based on the reordering equations of Passey & Henkes (2012) in panels A and B, Hemingway and Henkes (2021) in panels C and D, and Stolper and Eiler (2015) in panels E and F for two burial scenarios-shallower (left) and deeper (right), both assuming a typical geothermal gradient for the region of 25°C/km. Dark blue lines represent mean predicted evolution of $T_{\Delta47}$. All but one of the model-scenario combinations produce negligible reordering of $T_{\Delta47}$ (<+3°C).

PALEOSALINITY INFERENCES

Table S4. Calculations of bottomwater paleosalinity in the Cenomanian Western Interior Seaway (WIS) based on $\delta^{18}O_w$ measurements from clumped isotope analyses of oysters, using a wide range of scenarios for the oxygen isotope ($\delta^{18}O_w$) composition of freshwater runoff to the WIS. Calculations are reported in SI units for salinity. The values of WIS $\delta^{18}O_w$ derive from our measurements of Δ_{47} temperatures ($T_{\Delta47}$) and $\delta^{18}O_{carb}$ of fossil oyster powders and are presented as 95% confidence intervals on the standard error for unaltered Zones 1 and 3. "$\delta^{18}O_w$ (cal. Petersen et al.)" reflects $\delta^{18}O_w$ as calculated from $T_{\Delta47}$ values calibrated from the Petersen et al. (2019) equation and "$\delta^{18}O_w$ (cal. Anderson et al.)" reflects $\delta^{18}O_w$ as calculated from $T_{\Delta47}$ values calibrated using the Anderson et al. (2021) equation. Assumptions for the mixing equations include a salinity of runoff of 0 SI units and a salinity of 35 SI units for the marine water end member. The mean oceanic oxygen isotopic composition for the fully marine end member (δ_{ocean}) is assumed to be -1‰ (VSMOW) as originally proposed by Shackleton and Kennett (1975) for ice sheet-free geologic worlds. In tests of both more plausible and more extreme isotopic values for runoff (δ_{runoff}) (e.g., -30‰ vs -8‰ VSMOW), all scenarios reconstruct near-fully-marine to fully-marine benthic salinity conditions in the Cenomanian WIS.

WIS δ_w (‰VSMOW) **95% conf. interval**	runoff δ_{runoff} (salinity of 0 SI units)= -30‰ VSMOW marine δ_{ocean} (salinity of 35 SI units) = -1‰ VSMOW	runoff = -22‰ marine = -1‰	runoff = -11‰ marine = -1‰	runoff = -8‰ marine = -1‰
$\delta^{18}O_w$ (cal. Petersen et al.) **-0.9‰ to +0.1‰**	35.2 to 36.3 SI units	35.2 to 36.8 SI units	35.5 to 38.7 SI units	35.7 to 40.3 SI units
$\delta^{18}O_w$ (cal. Anderson et al.) **-1.4‰ to -0.5‰**	34.6 to 35.6 SI units	34.4 to 35.9 SI units	33.7 to 36.9 SI units	33.2 to 37.7 SI units

Note: In a sensitivity test, changing the marine δ_{ocean} value from -1‰ to 0‰ VSMOW shifted all salinity calculations by less than one SI unit (and by less than 0.3 SI unit in most scenarios).

LATE CRETACEOUS MARINE Δ_{47} DATA COMPILATION FOR NORTH AMERICA

Figure 4 in the main article displays a marine Δ_{47} data compilation from the Cretaceous North American Interior, including $T_{\Delta 47}$ and $\delta^{18}O_w$ from the Western Interior Seaway and the Mississippi Embayment. Raw data sources are Petersen et al. (2016), Meyer et al. (2018), Gao et al. (2021), and this study (Table S1h). Recently, Daëron et al 2016, Schauer et al 2016 and Petersen et al. (2019) documented that using updated parameters for the abundance of ^{17}O significantly affects the calculation of Δ_{47} values, and ultimately temperatures as well. Therefore, we have reprocessed all data from Petersen et al. (2016) utilizing the updated ^{17}O parameters of Brand et al. (2010). A similar reprocessing of data from Meyer et al. (2018) was performed by O'Hora et al. (in revision). In the case of the Campanian-Maastrichtian data in Petersen et al. (2016), the reprocessing systematically increased $T_{\Delta 47}$ by 6.6°C and $\delta^{18}O_w$ by 0.9‰ on average. A reprocessed version of "Supplementary Table S3" from Petersen et al. (2016) is available in Table S1h, along with Meyer et al. (2018) reprocessed data.

Supplementary references

Allan, J. R., and Matthews, R. K., 1982, Isotope signatures associated with early meteoric diagenesis: *Sedimentology*, v. 29, no. 6, p. 797-817, https://doi.org/10.1111/j.1365-3091.1982.tb00085.x.

Anderson, N.T. et al., 2021, A Unified Clumped Isotope Thermometer Calibration (0.5–1,100°C) Using Carbonate-Based Standardization: *Geophysical Research Letters*, v. 48, p. e2020GL092069, https://doi.org/10.1029/2020GL092069.

Bernasconi, S.M., Daëron, M., Bergmann, K. D., Bonifacie, M., Meckler, A. N., Affek, H. P., et al., 2021, InterCarb: A community effort to improve inter-laboratory standardization of the carbonate clumped isotope thermometer using carbonate standards: *Geochemistry, Geophysics, Geosystems*, 22, e2020GC009588. https://doi.org/10.1029/2020GC009588

Bonifacie, M., Calmels, D., Eiler, J.M., Horita, J., Chaduteau, C., et al., 2017, Calibration of the dolomite clumped isotope thermometer from 25 to 350 °C, and implications for a universal calibration for all (Ca, g, Fe)CO3 carbonates: *Geochimica et Cosmochimica Acta*, 200, p. 255-279, http://dx.doi.org/10.1016/j.gca.2016.11.028

Boudinot, F. G., Dildar, N., Leckie, R. M., Parker, A., Jones, M. M., Sageman, B. B., Bralower, T. J., and Sepúlveda, J., 2020, Neritic ecosystem response to Oceanic Anoxic Event 2 in the Cretaceous Western Interior Seaway, USA: *Palaeogeography, Palaeoclimatology, Palaeoecology*, v. 546, p. 109673, https://doi.org/10.1016/j.palaeo.2020.109673.

Bower, W.E., 1972, The Canaan Peak, Pine Hollow, and Wasatch Formations in the Table Cliff Region, Garfield County, Utah, Geological Survey Bulletin 1331-B, p. 39

Brand, W. A., Assonov, S. S., and Coplen, T. B., 2010, Correction for the 17O interference in δ(13C) measurements when analyzing CO2 with stable isotope mass spectrometry (IUPAC Technical Report): *Pure and Applied Chemistry*, v. 82, no. 8, p. 1719-1733, https://doi.org/10.1351/PAC-REP-09-01-05.

Burgener, L., Hyland, E., Huntington, K. W., Kelson, J. R., and Sewall, J. O., 2019, Revisiting the equable climate problem during the Late Cretaceous greenhouse using paleosol carbonate clumped isotope temperatures from the Campanian of the Western Interior Basin, USA: *Palaeogeography, Palaeoclimatology, Palaeoecology*, v. 516, p. 244-267, https://doi.org/10.1016/j.palaeo.2018.12.004.

Checa, A. G., Harper, E. M., and González-Segura, A., 2018, Structure and crystallography of foliated and chalk shell microstructures of the oyster Magallana: the same materials grown under different conditions: *Scientific Reports*, v. 8, no. 1, p. 7507, https://doi.org/10.1038/s41598-018-25923-6.

Cobban, W. A., 1977, Characteristic marine molluscan fossils from the Dakota Sandstone and intertongued Mancos Shale, west-central New Mexico: U.S. Geological Survey Open-File Report 1009, 30 p., https://pubs.usgs.gov/pp/1009/report.pdf.

Cochran, J. K., Kallenberg, K., Landman, N. H., Harries, P. J., Weinreb, D., Turekian, K. K., Beck, A. J., and Cobban, W. A., 2010, Effect of diagenesis on the Sr, O, and C isotope composition of late Cretaceous mollusks from the Western Interior Seaway of North America: *American Journal of Science*, v. 310, no. 2, p. 69, https://doi.org/10.2475/02.2010.01.

Crowley, P.D., Reiners, P.W., Reuter, J.M. Kaye, G.D., 2002, Laramide exhumation of the Bighorn Mountains, Wyoming: An apatite (U-Th)/He thermochronology study: *Geology*, v. 30, no.1, p. 27-30, https://doi.org/10.1130/0091-7613(2002)030%3C0027:LEOTBM%3E2.0.CO;2.

Daëron, M., Blamart, D., Peral, M., and Affek, H.P., 2016, Absolute isotopic abundance ratios and the accuracy of Δ47 measurements: *Chemical Geology*, v. 442, p. 83–96, https://doi.org/10.1016/j.chemgeo.2016.08.014.

de Winter, N. J., Vellekoop, J., Vorsselmans, R., Golreihan, A., Soete, J., Petersen, S. V., Meyer, K. W., Casadio, S., Speijer, R. P., and Claeys, P., 2018, An assessment of latest Cretaceous Pycnodonte vesicularis (Lamarck, 1806) shells as records for palaeoseasonality: a multi-proxy investigation: *Clim. Past*, v. 14, no. 6, p. 725-749, https://doi.org/10.5194/cp-14-725-2018.

Dennis, K. J., Affek, H. P., Passey, B. H., Schrag, D. P., and Eiler, J. M., 2011, Defining an absolute reference frame for 'clumped' isotope studies of CO2: *Geochimica et Cosmochimica Acta*, v. 75, no. 22, p. 7117-7131, https://doi.org/10.1016/j.gca.2011.09.025.

Elder, W. P., 1987, The Paleoecology of the Cenomanian-Turonian (Cretaceous) Stage Boundary Extinctions at Black Mesa, Arizona: *PALAIOS*, v. 2, no. 1, p. 24-40, https://doi.org/10.2307/3514570.

Elder, W. P., 1991, Molluscan paleoecology and sedimentation patterns of the Cenomanian-Turonian extinction interval in the southern Colorado Plateau region, in Nations, J. D., and Eaton, J. G., eds., Stratigraphy, depositional environments, and sedimentary tectonics of the Western Margin, Cretaceous Western Interior Seaway, Volume 260, Geological Society of America Special Paper, p. 113-137, https://doi.org/10.1130/SPE260-p113.

Fiebig, J., Hofmann, S., Löffler, N., Lüdecke, T., Methner, K., and Wacker, U., 2016, Slight pressure imbalances can affect accuracy and precision of dual inlet-based clumped isotope analysis: *Isotopes in Environmental and Health Studies*, v. 52, no. 1-2, p. 12-28, https://doi.org/10.1080/10256016.2015.1010531.

Flowers, R.M., Wernicke, B.P., and Farley, K.A., 2008, Unroofing, incision, and uplift history of the southwestern Colorado Plateau from apatite (U-Th)/He thermochronometry: *Geological Society of America Bulletin*, v. 120, p. 571–587, https://doi.org/10.1130/B26231.1.

Gao, Y., Henkes, G.A., Cochran, J.K., and Landman, N.H., 2021, Temperatures of Late Cretaceous (Campanian) methane-derived authigenic carbonates from the Western Interior Seaway, South Dakota, USA, using clumped isotopes: *Geological Society of America Bulletin*, v. 133, p. 2524–2534, https://doi.org/10.1130/B35846.1.

Hemingway, J. D. *isotopylog*: open-source tools for clumped isotope kinetic data analysis, http:pypi.python.org/pypi/isotopylog [online; accessed 2021-10-25]

Hemingway, J. D. and Henkes, G. A., 2021, A disordered kinetic model for clumped isotope bond reordering in carbonates: *Earth and Planetary Science Letters*, v. 566, 116962, https://doi.org/10.1016/j.epsl.2021.116962

Henkes, G. A., Passey, B. H., Grossman, E. L., Shenton, B. J., Pérez-Huerta, A., and Yancey, T. E., 2014, Temperature limits for preservation of primary calcite clumped isotope paleotemperatures: *Geochimica et Cosmochimica Acta*, v. 139, p. 362-382, https://doi.org/10.1016/j.gca.2014.04.040.

Henkes, G.A., Passey, B.H., Grossman, E.L., Shenton, B.J., Yancey, T.E., and Pérez-Huerta, A., 2018, Temperature evolution and the oxygen isotope composition of Phanerozoic oceans from carbonate clumped isotope thermometry: *Earth and Planetary Science Letters*, v. 490, p. 40–50, https://doi.org/10.1016/j.epsl.2018.02.001.

Hook, S., and Cobban, W., 1977, Pycnodonte newberryi (Stanton)--common guide fossil in Upper Cretaceous of New Mexico: New Mexico State Bureau of Mines and Mineral Resources Annual Report (July 1, 1976 to June 30,1977).

Hook, S. C. and Cobban, W. A., 1981, Late Greenhorn (mid-Cretaceous) discontinuity surfaces, southwest New Mexico, *in* Hook, S. C., ed., Contributions to mid-Cretaceous paleontology and stratigraphy of New Mexico: New Mexico Bureau of Mines and Mineral Resources, Circular 180, p. 5-21.

Huyghe, D., Emmanuel, L., de Rafelis, M., Renard, M., Ropert, M., Labourdette, N., and Lartaud, F., 2020, Oxygen isotope disequilibrium in the juvenile portion of oyster shells biases seawater temperature reconstructions: Estuarine, Coastal and Shelf Science, v. 240, p. 106777, https://doi.org/10.1016/j.ecss.2020.106777.

Jones, T. S., 1938, Geology of Sierra de la Pena and paleontology of the Indidura Formation, Coahuila, Mexico: *Geological Society of America Bulletin*, v. 49, no. 1, p. 69-150, https://doi.org/10.1130/GSAB-49-69.

Kauffman, E. G., 1967, Coloradoan macroinvertebrate assemblages, central Western Interior, United States, *in* Paleoenvironments of the Cretaceous seaway in the Western Interior; a symposium: Golden, Colorado, Colorado School of Mines, p. 67-144.

Kauffman, E. G. and Powell, J. D., 1977, Paleontology, *in* Kauffman, E.G., Hattin, D.E., and Powell, J.D., Stratigraphic, Paleontologic, and Paleoenvironmental analysis of the Upper Cretaceous rocks of Cimarron County, northwestern Oklahoma: Geological Society of America, Memoir 149, p. 47-141, https://doi.org/10.1130/MEM149-p47.

Kauffman, E. G., and Caldwell, W. G. E., 1993, The Western Interior Basin in space and time, in Caldwell, W. G. E., and Kauffman, E. G., eds., Evolution of the Western Interior Basin, Volume Special Paper 39, Geological Association of Canada, p. 1-30.

Kauffman, E. G., Sageman, B. B., Kirkland, J. I., Elder, W. P., Harries, P. J., and Villamil, T., 1993, Molluscan Biostratigraphy of the Cretaceous Western Interior Basin, North America, in Caldwell, W. G. E., and Kauffman, E. G., eds., Evolution of the Western Interior Basin, Volume 39, Geological Association of Canada, p. 397-434.

Kim, S.-T., and O'Neil, J. R., 1997, Equilibrium and nonequilibrium oxygen isotope effects in synthetic carbonates: *Geochimica et Cosmochimica Acta*, v. 61, no. 16, p. 3461-3475, https://doi.org/10.1016/S0016-7037(97)00169-5.

Kirby, M. X., Soniat, T. M., and Spero, H. J., 1998, Stable isotope sclerochronology of Pleistocene and Recent oyster shells (Crassostrea virginica): *PALAIOS*, v. 13, no. 6, p. 560-569, https://doi.org/10.2307/3515347.

Kirkland, J. I., 1996, Paleontology of the Greenhorn cyclothem (Cretaceous: late Cenomanian to middle Turonian) at Black Mesa, northeastern Arizona: *New Mexico Museum of Natural History and Science Bulletin*, v. 9, p. 1-131.

Knoll, K., Landman, N. H., Cochran, J. K., Macleod, K. G., and Sessa, J. A., 2016, Microstructural preservation and the effects of diagenesis on the carbon and oxygen isotope composition of Late Cretaceous aragonitic mollusks from the Gulf Coastal Plain and the Western Interior Seaway: *American Journal of Science*, v. 316, no. 7, p. 591, https://doi.org/10.2475/07.2016.01.

Lacroix, B. and Niemi, N. A., 2019, Investigating the effect of burial histories on the clumped isotope thermometer: An example from the Green River and Washakie Basins, Wyoming: *Geochimica et Cosmochimica Acta*, v. 247, p. 40-58, https://doi.org/10.1016/j.gca.2018.12.016.

Law, B.E., 1992, Thermal maturity patterns of Cretaceous and Tertiary rocks, San Juan Basin, Colorado and New Mexico: *Geological Society of America Bulletin*, v. 104, p. 192-207, https://doi.org/10.1130/0016-7606(1992)104%3C0192:TMPOCA%3E2.3.CO;2.

Lee, S.-W., Jang, Y.-N., Ryu, K.-W., Chae, S.-C., Lee, Y.-H., and Jeon, C.-W., 2011, Mechanical characteristics and morphological effect of complex crossed structure in biomaterials: Fracture mechanics and microstructure of chalky layer in oyster shell: *Micron*, v. 42, no. 1, p. 60-70, https://doi.org/10.1016/j.micron.2010.08.001.

Linzmeier, B. J., 2019, Refining the interpretation of oxygen isotope variability in free-swimming organisms: Swiss *Journal of Palaeontology*, v. 138, no. 1, p. 109-121, https://doi.org/10.1007/s13358-019-00187-3.

Lynds, R. M. and Slattery, J. S., 2017, Correlation of the Upper Cretaceous Strata of Wyoming, Wyoming State Geological Survey (2017), (Open File Report 2017–3)

McKinney, K.C., and Cobban, W.A., 2018, USGS Denver Mesozoic Catalog for 14595 fossil localities from the Rocky Mountain Region (1933-2017): U.S. Geological Survey data release, https://doi.org/10.5066/F7057F62.

Meyer, K. W., Petersen, S. V., Lohmann, K. C., and Winkelstern, I. Z., 2018, Climate of the Late Cretaceous North American Gulf and Atlantic Coasts: *Cretaceous Research*, v. 89, p. 160-173, https://doi.org/10.1016/j.cretres.2018.03.017.

Morrison, J. O., and Brand, U., 1988, An evaluation of diagenesis and chemostratigraphy of Upper Cretaceous molluscs from the Canadian Interior Seaway: *Chemical Geology*, v. 72, no. 3, p. 235-248, https://doi.org/10.1016/0168-9622(88)90027-9.

Murray, K.E., Reiners, P.W., Thomson, S.N., Robert, X., and Whipple, K.X., 2019, The thermochronologic record of erosion and magmatism in the Canyonlands region of the Colorado Plateau: *American Journal of Science*, v. 319, p. 339–380, https://doi.org/10.2475/05.2019.01.

Nadeau, P. H., and Reynolds, R. C., 1981, Burial and contact metamorphism in the Mancos Shale: *Clays and Clay Minerals*, v. 29, no. 4, p. 249-259, https://doi.org/10.1346/CCMN.1981.0290402.

Nuccio, V. F., Finn, T. M., and Johnson, R. C., 1996, Thermal maturity data used for the assessment of gas resources in the Wind River basin, Wyoming, 96-64.

Nuccio, V.F. and Condon, S.M., 1996, Burial and thermal history of the Paradox Basin, Utah and Colorado, and Petroleum Potential of the Middle Pennsylvanian Paradox Formation, *in* Huffman, A.C., Lund, W.R., and Godwin, L.H., eds., Geology and Resources of the Paradox Basin: Utah Geological Association Guidebook 25, p. 57-76.

O'Hora, H.E., Petersen, S.V., Vellekoop, J., Jones, M.M., and Scholz, S.R., 2021, Clumped-isotope-derived climate trends leading up to the end-Cretaceous mass extinction in northwest Europe: *Climate of the Past Discussions*, p. 1–28, https://doi.org/10.5194/cp-2021-104.

Pacheco, K.W., 2013, Petroleum Potential for the Gothic Shale, Paradox Formation in the Ute Mountain Ute Reservation, Colorado and New Mexico [M.S. thesis]: Colorado School of Mines, 83 p.

Pancost, R.D., Freeman, K.H., Arthur, M.A., 1998, Organic geochemistry of the Cretaceous Western Interior Seaway: A trans-basinal evaluation, *in* Arthur, M.A., and Dean, W.E., eds., Stratigraphy and Paleoenvironments of the Cretaceous Western Interior Seaway, USA, SEPM Concepts in Sedimentology and Paleontology No. 6, p. 173-188, https://doi.org/10.2110/csp.98.06.0173.

Parrish, J. T., Hyland, E. G., Chan, M. A., and Hasiotis, S. T., 2019, Stable and clumped isotopes in desert carbonate spring and lake deposits reveal palaeohydrology: A case study of the Lower Jurassic Navajo Sandstone, south-western USA: *Sedimentology*, v. 66, no. 1, p. 32-52, https://doi.org/10.1111/sed.12540.

Passey, B. H., and Henkes, G. A., 2012, Carbonate clumped isotope bond reordering and geospeedometry: *Earth and Planetary Science Letters*, v. 351-352, p. 223-236, https://doi.org/10.1016/j.epsl.2012.07.021.

Petersen, S. V., Defliese, W. F., Saenger, C., Daëron, M., Huntington, K. W., John, C. M., Kelson, J. R., Bernasconi, S. M., Colman, A. S., Kluge, T., Olack, G. A., Schauer, A. J., Bajnai, D., Bonifacie, M., Breitenbach, S. F. M., Fiebig, J., Fernandez, A. B., Henkes, G. A., Hodell, D., Katz, A., Kele, S., Lohmann, K. C., Passey, B. H., Peral, M. Y., Petrizzo, D. A., Rosenheim, B. E., Tripati, A., Venturelli, R., Young, E. D., and Winkelstern, I. Z., 2019, Effects of Improved 17O Correction on Interlaboratory Agreement in Clumped Isotope Calibrations, Estimates of Mineral-Specific Offsets, and Temperature Dependence of Acid Digestion Fractionation: *Geochemistry, Geophysics, Geosystems*, v. 20, no. 7, p. 3495-3519, https://doi.org/10.1029/2018GC008127.

Petersen, S. V., Tabor, C. R., Lohmann, K. C., Poulsen, C. J., Meyer, K. W., Carpenter, S. J., Erickson, J. M., Matsunaga, K. K. S., Smith, S. Y., and Sheldon, N. D., 2016, Temperature and salinity of the Late Cretaceous Western Interior Seaway: *Geology*, v. 44, no. 11, p. 903-906, https://doi.org/10.1130/G38311.1.

Rosenheim, B. E., Tang, J., and Fernandez, A., 2013, Measurement of multiply substituted isotopologues ('clumped isotopes') of CO2 using a 5 kV compact isotope ratio mass spectrometer: Performance, reference frame, and carbonate paleothermometry: *Rapid Communications in Mass Spectrometry*, v. 27, no. 16, p. 1847-1857, https://doi.org/10.1002/rcm.6634.

Ryb, U., Lloyd, M.K., and Eiler, J.M., 2021, Carbonate clumped isotope constraints on burial, uplift and exhumation histories of the Colorado Plateau: *Earth and Planetary Science Letters*, V. 566, 116964, https://doi.org/10.1016/j.epsl.2021.116964

Schauer, A.J., Kelson, J., Saenger, C., and Huntington, K.W., 2016, Choice of 17O correction affects clumped isotope (Δ47) values of CO2 measured with mass spectrometry: *Rapid Communications in Mass Spectrometry*, v. 30, p. 2607–2616, https://doi.org/10.1002/rcm.7743.

Sealey, P. L., and Lucas, S. G., 2003, Exceptionally preserved invertebrate fauna from the Upper Cretaceous Paguate Member of the Dakota Formation, Rio Puerco Valley, New Mexico: New Mexico Geological Society Guidebook, v. 54th Field Conference, Geology of the Zuni Plateau, p. 331-337.

Shackleton N.J. Kennett J.P., 1975, Paleotemperature history of the Cenozoic and the initiation of Antarctic glaciation: Oxygen and carbon isotope analysis in DSDP Sites 277, 279, and 280, in Kennett J.P., et al, Initial reports of the Deep Sea Drilling Project, Volume 29: Washington, D.C., U.S. Government Printing Office, p. 743–755, doi:10.2973/dsdp.proc.29.117.1975.

Stanton, T. W., 1893, The Colorado formation and its invertebrate fauna: U.S. Geological Survey Bulletin, v. 106, pp. 1-288, https://doi.org/10.3133/b106.

Stolper, D. A., and Eiler, J. M., 2015, The kinetics of solid-state isotope-exchange reactions for clumped isotopes: A study of inorganic calcites and apatites from natural and experimental samples: *American Journal of Science*, v. 315, no. 5, p. 363-411, https://doi.org/10.2475/05.2015.01.

Suarez, M. B., Knight, J. A., Godet, A., Ludvigson, G. A., Snell, K. E., Murphy, L., and Kirkland, J. I., 2020, Multiproxy strategy for determining palaeoclimate parameters in the Ruby Ranch Member of the Cedar Mountain Formation: *Geological Society, London, Special Publications*, v. 507, p. SP507-2020-2085, https://doi.org/10.1144/SP507-2020-85.

Surge, D., Lohmann, K. C., and Dettman, D. L., 2001, Controls on isotopic chemistry of the American oyster, Crassostrea virginica: implications for growth patterns: *Palaeogeography, Palaeoclimatology, Palaeoecology*, v. 172, no. 3, p. 283-296, https://doi.org/10.1016/S0031-0182(01)00303-0.

Titschack, J., Zuschin, M., Spötl, C., and Baal, C., 2010, The giant oyster *Hyotissa hyotis* from the northern Red Sea as a decadal-scale archive for seasonal environmental fluctuations in coral reef habitats: *Coral Reefs*, v. 29, no. 4, p. 1061-1075, https://doi.org/10.1007/s00338-010-0665-7.

Titus, A. L., Powell, J. D., Roberts, E. M., Sampson, S. D., Pollock, S. L., Kirkland, J. I., and Albright, B. L., 2005, Late Cretaceous stratigraphy, depositional environments, and macrovertebrate paleontology of the Kaiparowits Plateau, Grand Staircase–Escalante National Monument, Utah, in Pederson, J., and Dehler, C. M., eds., Interior Western United States, Volume 6, Geological Society of America Field Guide, p. 101-128, https://doi.org/10.1130/2005.fld006(05).

Todes, J., Jones, M. M., Sageman, B. B., and Osburn, M. R., 2017, A Compound-Specific Hydrogen Isotope Record at the Onset of Ocean Anoxic Event 2, Kaiparowits Plateau, Southern Utah, Fall Meeting 2017: San Francisco, CA, American Geophysical Union, p. PP23A-2251.

Ullmann, C. V., Böhm, F., Rickaby, R. E. M., Wiechert, U., and Korte, C., 2013, The Giant Pacific Oyster (Crassostrea gigas) as a modern analog for fossil ostreoids: Isotopic (Ca, O, C) and elemental (Mg/Ca, Sr/Ca, Mn/Ca) proxies: *Geochemistry, Geophysics, Geosystems*, v. 14, no. 10, p. 4109-4120, https://doi.org/10.1002/ggge.20257.
Ullmann, C. V., Wiechert, U., and Korte, C., 2010, Oxygen isotope fluctuations in a modern North Sea oyster (Crassostrea gigas) compared with annual variations in seawater temperature: Implications for palaeoclimate studies: *Chemical Geology*, v. 277, no. 1, p. 160-166, https://doi.org/10.1016/j.chemgeo.2010.07.019.
Veizer, J., 1983, Chemical diagenesis of carbonates: Theory and application of trace element technique, in Arthur, M. A., and Andersen, T. F., eds., Stable Isotopes in Sedimentary Geology, Volume 10: Tulsa, SEPM Short Course, p. 1-100, https://doi.org/10.2110/scn.83.01.0000.
Voigt, S., Wilmsen, M., and Mortimore, R. N., 2003, Cenomanian palaeotemperatures derived from the oxygen isotopic composition of brachiopods and belemnites: evaluation of Cretaceous palaeotemperature proxies: *International Journal of Earth Sciences*, v. 92, no. 2, p. 285-299, https://doi.org/10.1007/s00531-003-0315-1.
Wang, Z., Schauble, E. A., and Eiler, J. M., 2004, Equilibrium thermodynamics of multiply substituted isotopologues of molecular gases: *Geochimica et Cosmochimica Acta*, v. 68, no. 23, p. 4779-4797, https://doi.org/10.1016/j.gca.2004.05.039.